# Journal of Applied Sciences

ISSN 1812-5654

science alert

ANSInet
an open access publisher
http://ansinet.com

Journal of Applied Sciences 12 (24): 2534-2540, 2012
ISSN 1812-5654 / DOI: 10.3923/jas.2012.2534.2540


# Characteristics of Induction Flow in SI Direct Injection Engine with Dual Variable Swirl Control Valve

Yohannes T. Anbese, A. Rashid A. Aziz and Morgan R. Heikal
Center for Automotive Research and Electric Mobility, Universiti Teknologi PETRONAS,
Bandar Seri Iskandar, 31750 Tronoh, Perak, Malaysia

**Abstract:** The flame development and propagation in a SI engine is highly influenced by the level and structure of the flow turbulence near the spark plug. These turbulent characteristics near the time of combustion are the result of the induction and compression processes. The main source of turbulent kinetic energy in the engine is the induction process. This study investigates the swirl characteristics of the induction process using a Particle Image Velocimetry (PIV) system and an experimental rig of an actual cylinder head and a transparent acrylic cylinder liner. Three induction cases with different swirl valve settings were selected. The intake valve lift was adjusted in steps of 1 mm to a maximum opening of 7 mm. PIV images were collected at each swirl adjustment and each valve lift to acquire average velocity vector fields. The total velocity field was decomposed into large-scale and small-scale components using the LES homogeneous decomposition technique. The result shows that coherent and organized swirling cores were formed when the Swirl Control Valve (SCV) was partially closed. The vortex core at 50° SCV setting was compact and strong compared to the higher degree adjustment (90°). There was no clear organized swirling flow structure in the swirl plane in the case of full-open SCV induction, but a number of clockwise and counter clockwise vortices were observed. However, for this case, the small-scale vortex field analysis showed that breaking-up of the macrostructure occurred at a higher rate than in the partially-open cases.

**Key words:** Induction flow, vortex flow, swirl flow, swirl number, PIV data model

## INTRODUCTION

Popularity of direct injection spark ignition engines are increasing due to their economical fuel consumption with lean fuel stratification technique. In such type of combustion system (especially with a late fuel injection) the charge flow inside the cylinder should acquire sufficient turbulence to create combustible mixture and faster flame development. Such kind of turbulent flow in the cylinder is achieved mainly from the kinetic energy held by the induction flow and to some extent due to the motion of the piston during the compression process.

Two main in-cylinder flow structures are commonly known for IC engines, swirl and tumble. A swirling intake is the flow that rotates about the cylinder axis, whereas a tumble flow has a rotation axis that is perpendicular to the cylinder axis. Today, a combined swirl and tumble flows are commonly used in engines. The magnitude of the generated swirl and/or tumble flows is highly dependent on the engine geometries such as intake port design, bore/stroke ratio and cylinder head shape (Heywood, 1988). Different measurement techniques, from the hot-wire anemometer (Pajkovic and Petrovic, 2008) to the time resolved PIV using high frequency laser and high frame rate cameras. Pust (2003) have been used to understand the flow inside the cylinder. Though higher time resolution can be obtained using Hot-wire Anemometer (HWA) and Laser Doppler Velocimetry (LDV) (Oyewola, 2006), the PIV technique becomes popular due to its planner measurement capability. Josefsson *et al*. (2001) utilized both LDV and PIV techniques to measure the integral scale and turbulence intensity in a motored SI engine. The result they obtained using PIV technique was similar to the LDV one. They showed the importance of the PIV method for flow measurement compared to the well-established LDV method. However, there are some limitations with the PIV technique. These are (1) very difficult to acquire time resolutions due to lower laser pulse repetition and lower camera frame rates; (2) the maximum spatial resolution is also limited by the size of the interrogation window. Recently, high pulsing rate Nd:YAG and Nd:YLF lasers that can have repetition rates

**Corresponding Author:** Yohannes T. Anbese, Center for Automotive Research and Electric Mobility, Universiti Teknologi PETRONAS, Bandar Seri Iskandar, 31750 Tronoh, Perak, Malaysia

in kHz and imaging devices with thousands of frames per second are available for high speed PIV flow measurements. However, the pulse energy drops exponentially with increasing repetition rate as discussed (Pust, 2003) and that could affect the quality of the data. On the other hand numerical modeling using sophisticated CFD codes is also a common practice as processing speed and capacity of computers enhanced (Kurniawan *et al*., 2007; Lashkarpour *et al*., 2011). This part, however, is not considered in the scope of the current study. Though the main source of turbulence inside cylinder is from the induction process, some contribution of the compression process was recorded by Kang and Baek (1998). Since viscous shear stresses are performing continuous deformation of the fluid layers that converts turbulent kinetic energy into internal energy (Pope, 2000), this makes turbulent flow always dissipative and so unless otherwise there is a continuous source of energy to generate turbulence, it eventually decays. Turbulent decaying was observed even before the inlet valves were closed (Funk, 2005). Nonetheless, the decaying rate is highly dependent on the intake flow structure. Lower rates of decay were reported in swirling inductions compared to the tumble one due to the geometry of the cylinder that can be favorable for the swirling flow structure to preserve its kinetic energy and experience a lesser rate of viscous dissipation than the tumble structure (Heywood, 1988; Zhao *et al*., 2002). In most SI engines, intake ports are designed to have a tumble induction due to the faster breakdown rate of tumble flow structure inside the cylinder. In a recent study, Lee *et al*. (2007) identified the existence of a correlation between strong tumble and turbulence level at the time of ignition. However, in lean operation, they observed that combined swirl and tumble intake provided a rapid and stable combustion. In addition to the nature of induction flows, combustion chamber geometry and engine speed also affect the turbulent flow structures inside the cylinder as discussed (Krishna and Mallikarjuna, 2009). Generally, previous works clearly showed that knowledge of in-cylinder flow was critical to study combustion processes in IC engines. The in-cylinder flow is highly influenced by the type of induction. Besides, the induction process is the source of kinetic energy for the bulk flow inside the cylinder. Therefore, it is important to investigate the nature of the induction flow structure of IC engines and incorporate it with the combustion and flame characteristic study. The current experimental study aimed to analyze the induction flow structure by creating combined swirl/tumble inductions at different levels in a steady state flow-rig using cylinder head of the actual engine and a transparent acrylic chamber that mimics the engine cylinder liner. This practice can be helpful to visualize induction flows in non-optical engines.

## MATERIALS AND METHODS

**Experimental facilities and procedures:** The experimental setup is shown briefly in Fig. 1. It consisted of cylinder head (taken from the CNG DI engine discussed (Anbese *et al*., 2011), an optical cylinder made of 3 mm thick acrylic glass having the same bore and stroke dimensions of the engine cylinder liner, 45° mirror arrangement for swirl plane visualization through the bottom of the cylinder, a metallic structural frame to support the head and the cylinder, blower for air supply and a PIV system for flow data acquisition and data analysis. The PIV image recording was achieved using 12 bit HiSence CCD camera with a full resolution of 1280×1024 pixels. In a double-frame cross-correlation PIV flow recording, its maximum frame rate reached up to 4.5 Hz. Illumination of seed particles in the flow was realized using a Q-switched double-pulsed Nd: YAG Gemini 200 laser. The laser system consisted of two cavities for generation of dual laser pulses at 532 nm wavelength having 200 mJ of energy and 15 Hz generation frequency. The duration of each pulse and the time between the pulses were set to be 10 ns and 100 μsec, respectively. The cylinder head had four valves (two intake and two exhaust) and the SCV was attached to the intake port. The port was originally designed for a tumble intake flow capability. Later on, it was modified by inserting a Swirl Control Valve (SCV) device having two

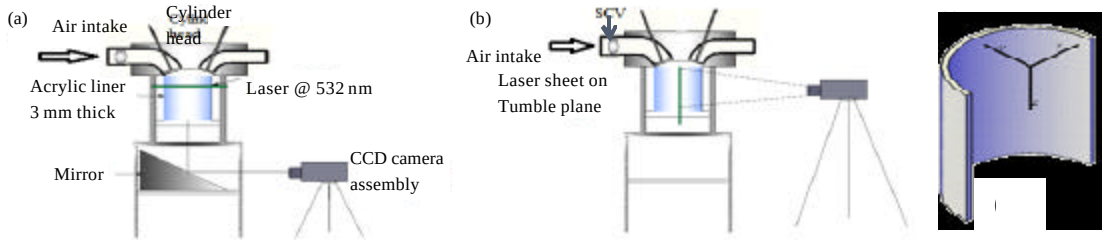


Fig. 1(a-c): PIV setup (a) Swirl plane, (b) Tumble plane and (c) Flow coordinate axis in the cylinder


Fig. 2(a-c): Swirl control valves arrangement for the three different induction cases (a) Case I, (b) Case II and (c) Case III

Table 1: Swirl control valve adjustment angles and their designation

| | SCV closure adjustment | |
|---|---|---|
| Induction type | left | right |
| Case-I | 10 deg closure | 10 deg closure |
| Case-II | 50 deg closure | 10 deg closure |
| Case-III | 90 deg closure | 10 deg closure |

separately adjustable flaps that guided the flow through the valves into the cylinder in a swirling motion pattern.

The analysis of flow characteristics during induction on this new setup for the variable induction strategy was achieved by varying the intake valve openings at different valve lift positions. A valve lock was fabricated and used to maintain the opening at the target lift position. When the valve reached the maximum lift, it was measured to be 7 mm from the seat. Therefore, the valve opening was divided into seven hold points so that flow data would be captured every 1 mm lift. The procedure was, first to set the valve lift position then vary the SCV closure adjustment and gathering PIV data on the swirl and tumble planes. Three different induction cases were selected by adjusting the left flap of the SCV only, as demonstrated in Fig. 2. The different induction types and the respective SCV adjustments are summarized in Table 1.

**PIV data analysis:** PIV images were captured at each SCV setting and intake valve position. These sequential image frames were sub-sampled into smaller regions called interrogation areas of size 64×64 pixels. Cross-correlation between the two frames was performed using the Dantec FlowManager software, applying Fast Fourier Transform (FFT) algorithm for a robust correlation.

Image enhancement actions were taken to minimize correlation errors due to variations in signal intensities as suggested by Raffel *et al.* (2007). These procedures included background subtraction, masking of unwanted regions and applying Gaussian weighting function to suppress the influence of edge signals.

After correlation and validation of the vector data, the local swirl strength of the induction flow was identified and located in the flow field using the local velocity gradient tensor and the corresponding eigenvalue (Adrian *et al.*, 2000; Hutchins *et al.*, 2005) given by:

$$\begin{bmatrix} \frac{\partial u}{\partial x}-\lambda & \frac{\partial v}{\partial x} \\ \frac{\partial u}{\partial y} & \frac{\partial v}{\partial y} \end{bmatrix}=0 \quad (1)$$

where, u and v are the x and y velocity components, respectively. $\lambda$ is the eigenvalue.

The magnitude of the swirling strength of the vortex was then identified from the imaginary part of the eigenvalue, $\lambda_1$ as detailed by Adrian *et al.* (2000) and Hutchins *et al.* (2005):

$$\lambda_1=\frac{1}{2}\sqrt{\left|\left(\frac{\partial u}{\partial x}+\frac{\partial v}{\partial y}\right)^2-4\left(\frac{\partial u}{\partial x}\frac{\partial v}{\partial y}-\frac{\partial u}{\partial y}\frac{\partial v}{\partial x}\right)\right|} \quad (2)$$

The swirling direction was found by analyzing the surrounding velocity field as suggested by Raffel *et al.* (2007) and multiplying $\lambda_1$ by the sign of the local vorticity as used in by Hutchins *et al.* (2005). Hence, the strength of the swirling vortex and its direction of rotation was obtained from:

$$\lambda_S=\lambda_1\frac{|\omega_z|}{\omega_z} \quad (3)$$

where, $\omega_Z$ is the local vorticity.

## RESULTS AND DISCUSSION

**Swirl plane flow visualization:** The swirling flows were created around the valve stem inside the port due to deflection of the flow by the adjustable disc in the SCV device. The swirling flow observations were carried out at two selected swirl planes, 10 and 40 mm downstream from the valve seats as shown in Fig. 3. Swirling vortices on the 10 mm plane were noticed from the air coming through the adjusted portion of the SCV only in the second and third induction cases as shown in Fig. 4. The 10° adjustment of the SCV in Case-I created no swirling vortex and so it was considered as a medium-tumble induction rather than a swirl induction.

The small-sized circulating vortices observed near the left valve seat increased their core size downstream in the cylinder and inclined towards the other side of the

cylinder. Figure 5 depicts streamlines and swirl velocity vector field at the maximum valve lift (7 mm) for the three induction cases at the swirl plane 40 mm downstream from the valve seats. The shape of the circulating flows observed at the two swirl inductions was different from each other. The 50° closed SCV (Case-II induction) showed strong and compact core compared to the 90°closed one (Case-III induction). Regarding vortex core size, Case-III induction acquired the largest size; however,

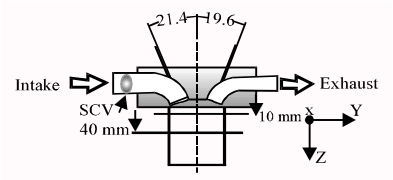


Fig. 3: Intake valve and SCV position in the port

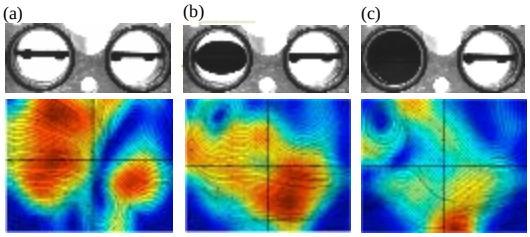


Fig. 4(a-c): SCV adjustments and the respective flow streamlines for (a) Case-I , (b) Case-II and (c) Case-III inductions at a swirl plane 10 mm downstream from valve seats

the local swirl strength was dispersed and weaker over the surface of the core, as shown in Fig. 5. The core center also showed an offset from the center of the ellipse-like swirling vortex structure along its major axis. Since the SCV flaps adjustment of the two divided intake ports were different, as demonstrated in Fig. 2, the swirling vortices created by the 90° closed portion of the SCV in Case-III seemed to be distorted and eroded by the relatively strong tumble-like flow from the 10° closed portion of the SCV (right portion of the intake port). The swirling vortices observed in both the second and third induction cases were coherent and clearly seen in almost all valve lift positions.

**Swirl velocity fluctuations and flow structures:** Figure 6a-c shows the profile of velocity measured on the 40 mm swirl plane (along the center line of the plane) for the variable induction cases at different valve lifts, while Fig. 6d shows the same velocity profile at maximum valve lift (7 mm). The legends in the figures indicate the induction type and level of valve opening. For instance, CI-4 means Case-I induction at 4 mm valve lift. In all cases of valve lift, strong spatial fluctuations of swirl velocity along the measurement line were observed due to the existence of vortices on the sampled swirl plane. The magnitude of the swirl velocity increased with valve lifts in all induction cases. The lower and upper peaks of the velocity profiles shown in the figures demonstrated the existence of vortices on the measurement plane as velocity magnitude dropped from the periphery towards

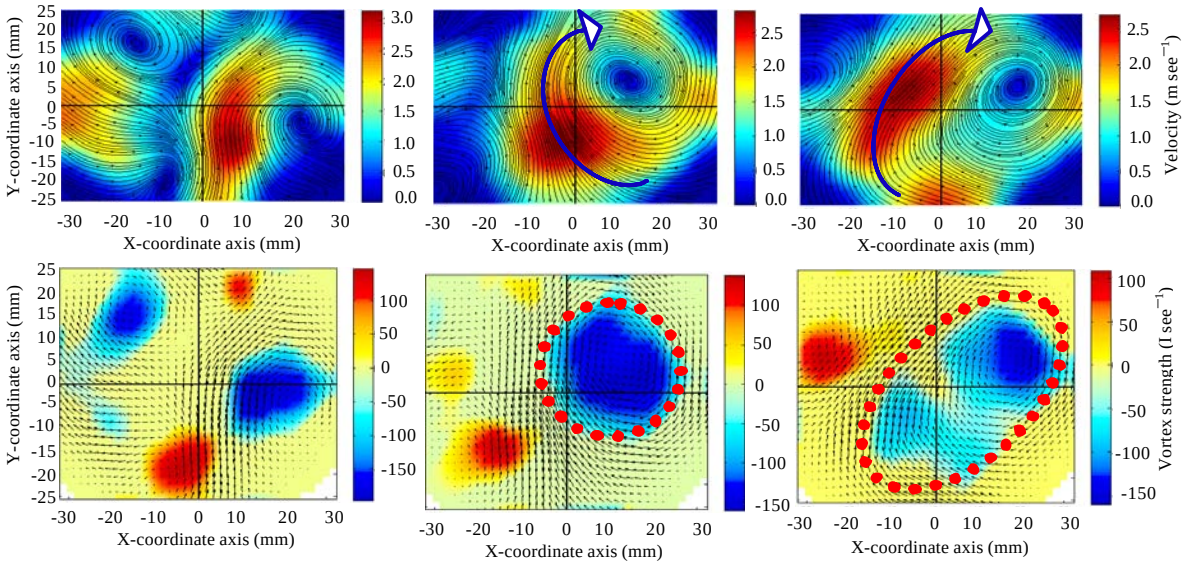


Fig. 5: Streamlines and local swirl strength maps at the 40 mm swirl plane for Case-I (left column), Case-II (middle column) and Case-III (right column)

Table 2: Variable SCV adjustments and induction flow characteristics

| Induction type | SCV adjustment angle | | Intake flow structure | Swirl number at max valve lift | Max RMS at 7 mm valve lift (m sec$^{-1}$) |
|---|---|---|---|---|---|
| | Left valve | Right valve | | | |
| CASE-I | 10° closed | 10° closed | Medium Tumble | - | 3.5 |
| CASE-II | 50° closed | 10° closed | Medium Swirl | 0.406 | 2.5 |
| CASE-III | 90° closed | 10° closed | High Swirl | 0.474 | 2.0 |

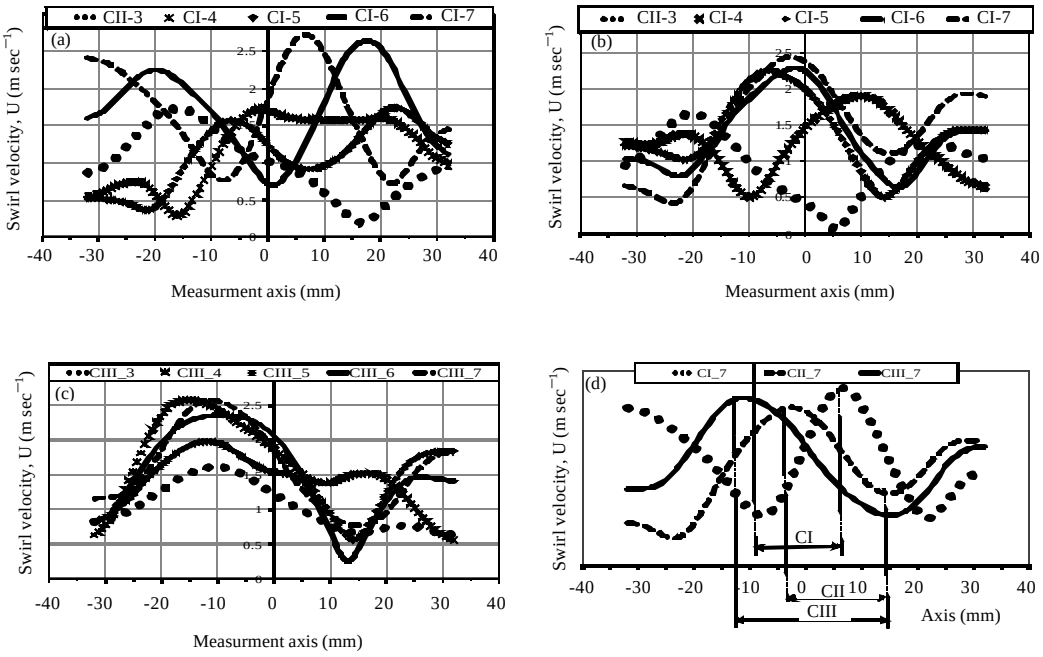


Fig. 6(a-d): Velocity profile (a-c) Along a Line y = 0 on a Swirl plane of 40 mm down from valve seats in the cylinder for the three different induction cases extracted from the vector fields and (d) At maximum valve lift (7 mm)

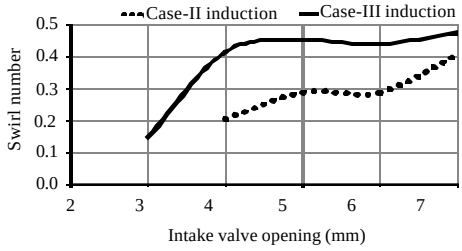


Fig. 7: Swirl number variation with valve lift

the vortex core center. The profiles might be useful to identify the number of swirling vortices and their core sizes on the plane. Due to the existence of multiple vortices in Case-I induction, velocity fluctuations along the measurement plane were observed to be high as shown in Fig. 6a. The vortex core size can be measured as the distance between the maximum swirl velocity location at the periphery of the core and the minimum velocity that was located at the center of the core as discussed (Paik *et al*., 2007). Figure 6d shows the profile of the swirl velocity at 7 mm valve lift for all cases of inductions. It was shown that the third induction case acquired the highest swirl core sizes of all cases. Estimated values of the core sizes taken from Figure 6d for Case-II and Case-III were about 26 and 20 mm, respectively. This showed that the vortex created by the swirling flow half way in the cylinder (on the 40 mm observation plane) acquired a core size of about one-third of the cylinder diameter. The size of vortex cores created by the swirling velocity was observed having a direct relation to the closure angle of the flaps in the SCV device (Table 2).

The swirl number, a dimensionless number used to characterize swirl intensity, was one of the parameters taken under consideration. It was identified from the ratio of the tangential and axial moments of momentum, as discussed (Crnojevic *et al*., 1999), for Case-II and Case-III inductions and plotted on Fig. 7. The swirling axis considered was the axis that passed through the center of the swirl core. It was found that the swirl intensity increased with intake valve opening, as it was also reported (Kang and Reitz, 2000); and Case-III induction with the maximum SCV closure

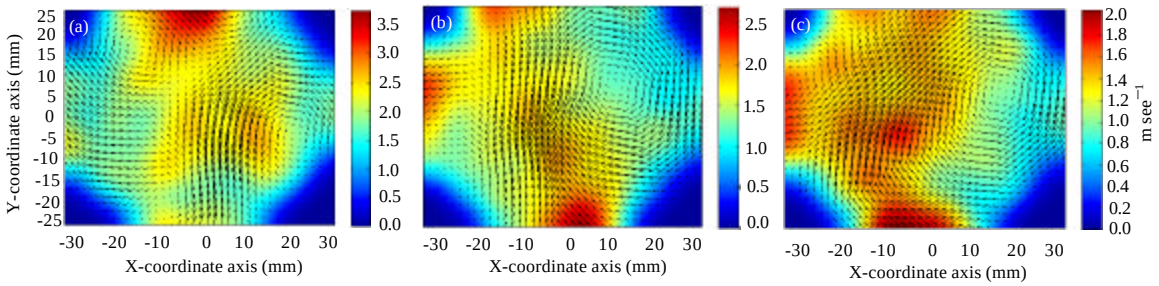


Fig. 8(a-c): RMS velocity fields for (a) Case I, (b) Case II and (c) Case III

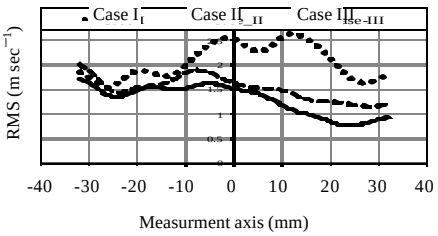


Fig. 9: RMS values on horizontal axis y = 0

acquired the highest swirl number. Since there was no coherent and structured swirling flow in Case-I induction (Fig. 5) identification of swirl number was not considered.

The root-mean-square (RMS) velocity fluctuation was the other flow parameter to be considered in this study. Figure 8 shows the RMS values of in-cylinder flows on the swirl plane at the three variable induction cases. In Case-I high RMS values were observed along the axis from the intake side of the cylinder portion to the exhaust side.

Whereas, in the other two induction cases, high RMS values dominated the left side of the cylinder (at the opposite side of the plane where the swirl core was located). High swirl strength region acquired low RMS values, whereas high velocity fluctuations (RMS) were observed on regions where high velocity values were recorded. The maximum calculated RMS values on the swirl plane of the three different inductions were observed declining with increasing SCV closure angles as shown in Fig. 8. Case-I with a 10° SCV flap closure exhibited about 3.5 m sec$^{-1}$ as its maximum, whereas the maximum value in case-II and Case-III inductions was 2.5 and 2 m sec$^{-1}$, respectively. Variations of RMS values with the variable inductions could be related to the nature of vortices formed on the swirl plane. Scattered and non-coherent vortices on the observed plane of the first induction case (which was considered to be medium-tumble) demonstrated higher velocity fluctuations. Though the other two induction cases showed coherent swirling vortices the one with the largest core size depicted the lowest fluctuation. The RMS values identified on a horizontal axis at y = 0 also supported the claim that larger swirling core had lower velocity fluctuations as depicted in Fig. 9.

Therefore, from the different parametric analysis on the swirl plane of the in-cylinder flow discussed previously, flow characteristics of the three variable inductions were summarized and tabulated in Table 2.

## CONCLUSION

The induction flow characteristics of an SI direct injection engine were analyzed in a separate experimental setup outside the engine by adjusting the closure angles of the SCV flaps separately. The PIV data analysis on the swirl plane showed that an increase in closure of the swirl control device enhanced the swirl intensity. However, the RMS values were found to be highest at a 10° closure SCV induction rather than at the higher closures (i.e. Case-II and Case-III inductions). The flow regions with strong swirl strength showed lower velocity fluctuations and RMS values on the swirl plane were associated with velocity magnitudes.

## REFERENCES

Adrian, R.J., K.T. Christensen and Z.C. Liu, 2000. Analysis and interpretation of instantaneous turbulent velocity fields. Exp. Fluids, 29: 275-290.

Anbese, Y.T., A.R.A. Aziz and Z.A.B.A. Karim, 2011. Flame development study at variable swirl level flows in a stratified CNG DI combustion engine using image processing technique. J. Applied Sci., 11: 1698-1706.

Crnojevic, C., F. Decool and P. Florent, 1999. Swirl measurements in a motor cylinder. Exp. Fluids, 26: 542-548.

Funk, C.O., 2005. An in-depth comparison of experimental and computational turbulence parameters for in-cylinder engine flows. Ph.D. Thesis, Department of Mechanical Engineering, University of Michigan, USA.

Heywood, J.B., 1988. Internal Combustion Engine Fundamentals. McGraw-Hill, New York.

Hutchins, N., W.T. Hambleton and I. Marusic, 2005. Inclined cross-stream stereo particle image velocimetry measurments in turbulent boundary layers. J. Fluid Mech., 541: 21-54.

Josefsson, G., J. Fischer and I. Magnusson, 2001. Length scale measurements in an engine using PIV and comparison with LDV. Proceedings of 5th International Symposium on Diagnostics and Modeling of Combustion in IC Engines, July 1-4, 2001, Nagoya, Japan, pp: 653-660.

Kang, K.Y. and J.H. Baek, 1998. Turbulence characteristics of tumble flow in a four-valve engine. Exp. Ther. Fluid Sci., 18: 231-243.

Kang, K.Y. and R.D. Reitz, 2000. Intake flow structure and swirl generation in a four-valve heavy-duty diesel engine. J. Eng. Gas Turbine Power, 122: 570-578.

Krishna, B.M. and J.M. Mallikarjuna, 2009. Tumble flow analysis in an unfired engine using particle image velocimetry. World Acad. Sci. Eng. Technol., 54: 430-435.

Kurniawan, W.H., S. Abdullah and A. Shamsudeen, 2007. A computational fluid dynamics study of cold-flow analysis for mixture preparation in a motored four-stroke direct injection engine. J. Applied Sci., 7: 2710-2724.

Lashkarpour, S.M., K. Bahlouli, S.E. Razavi and S.M. Milani, 2011. Experimental and computational investigation of effects of cooling intake air in $NO_x$, reduction and performance of diesel engines. Asian J. Applied Sci., 4: 30-41.

Lee, K., C. Bae and K. Kang, 2007. The effect of tumble and swirl flows on flame. Propagation in a four-valve S.I. engine. Applied Ther. Eng., 27: 2122-2130.

Oyewola, O.M., 2006. LDV measurements in a perturbed turbulent boundary layer. J. Applied Sci., 6: 2952-2955.

Paik, B.G., J. Kim, Y.H. Park and K.S. Kim, 2007. Investigation on the vortex structure of propeller wake influenced by loading on the blade. J. Mar. Sci. Technol., 12: 72-82.

Pajkovic, V.R. and S.V. Petrovic, 2008. Spatial flow velocity distribution around an inlet port/valve annulus. Thermal Sci., 12: 73-83.

Pope, S.B., 2000. Turbulent Flows. 6th Edn., Cambridge University Press, New York, ISBN-13: 9780521598866, Pages: 806.

Pust, O., 2003. Time resolved PIV solution. Proceedings of 12th International Conference on Fluid Flow Technologies, September 3-6, 2003, Budapest, Hungary, pp: 1-5.

Raffel, M., C.E. Willert, S.T. Wereley and J. Kompenhans, 2007. Particle Image Velocimetry: A Practical Guide. 2nd Edn., Springer, Berlin, Germany.

Zhao, F., D.L. Harrington and M.C.D. Lai, 2002. Automotive Gasoline Direct-Injection Engines. SAE International, Warrendale, Pennsylvania, USA.